



# A Concise Hysteretic Model of 590 N/mm<sup>2</sup> Grade High Performance Steel Considering the Bauschinger Effect

Satoshi Yamada<sup>1</sup> · Yu Jiao<sup>2</sup> · Dong-Seok Lee<sup>3</sup> · Takanori Ishida<sup>4</sup> · Shoichi Kishiki<sup>4</sup>

Received: 1 February 2020 / Accepted: 1 September 2020 / Published online: 10 September 2020  
© Korean Society of Steel Construction 2020

## Abstract

A concise hysteretic model of 590 N/mm<sup>2</sup> grade high performance steel SA440 which is used in Japan for building structure is proposed. First, cyclic loading tests of steel components under constant and programmed strain amplitude are performed. Then, hysteresis characteristics are modeled by decomposing the hysteresis curve into the skeleton part, Bauschinger part and the elastically unloading part. The skeleton part and the Bauschinger part are modeled by using the monotonic test result and bi-linear model, respectively. The proposed model is examined by comparing with test results. In addition, a series of member analysis is conducted with proposed model as for the example of application.

**Keywords** Hysteretic model · Bauschinger effect · High-performance steel

## 1 Introduction

In order to evaluate plastic deformation capacity of structural members subjected to random cyclic load such as seismic force, it is important to understand the hysteretic behavior of steel materials subjected to random cyclic loading. So far, many researches have been conducted to propose the hysteretic model of steel materials under cyclic loading (Ramberg and Osgood 1943; Menegotto and Pinto 1973, etc.). Such hysteretic model proposed has been usefully applied to analytical approaches. However, the uncertainties of the parameters are difficult to determine. In addition, in case of complicated model such as Ramberg–Osgood model and Menegotto–Pinto model, the mathematical relationship is not convenient for use for simplified analysis with custom made program.

In the previous studies (Kato et al. 1970, 1973; Akiyama 1985), it has been clearly demonstrated that the hysteresis loops under cyclic loading of steel material and members can be decomposed into the skeleton part, the Bauschinger part and the elastic unloading part. Moreover, the shape of the skeleton curve obtained by connecting the skeleton parts, is similar to that of the monotonic loading curve. With this concept, a concise bi-linear model of the Bauschinger part for hysteretic model under arbitrary cyclic loading of structural members has been proposed (Akiyama et al. 1995). As for the steel material, a concise hysteretic model considering the Bauschinger effect of 400 N/mm<sup>2</sup> grade structural steel SS400B (JIS 3101 2010) and SN400B (JIS 3106 2012) was also proposed (Yamada and Jiao 2016). The practicability of the proposed hysteretic model was confirmed by comparing the analytical results of numerical in-plane beam analysis to experimental results of steel beam subjected to various loading histories.

The hysteretic behavior (stress–strain relationship and deformation capacity, etc.) of high performance steel is considered to be different from that of common structural steel. With the increased application of high performance steel, practical hysteretic models are necessary to simulate the structural behavior in structural analysis. Unfortunately, there is no such model for the 590 N/mm<sup>2</sup> grade high performance steel SA440 (JISF 2004). Therefore, in this study, a concise hysteretic model of SA440 is proposed using the same concept of previous study based on the cyclic loading

✉ Yu Jiao  
yjiao.sjtu.titech@gmail.com

<sup>1</sup> Department of Architecture, The University of Tokyo, Tokyo 113-8656, Japan

<sup>2</sup> Faculty of Engineering, Tokyo City University, Tokyo 158-8557, Japan

<sup>3</sup> Hyundai Steel (Former Tokyo Institute of Technology), Dangjin-si 31719, Korea

<sup>4</sup> Institute of Innovative Research, Tokyo Institute of Technology, Yokohama 226-8503, Japan

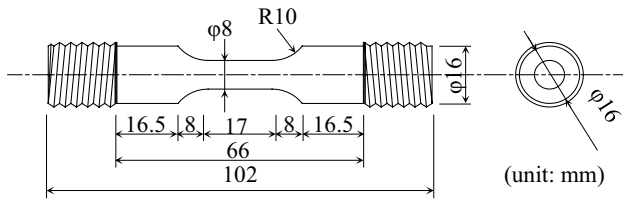


Fig. 1 Geometry of the specimen

Table 1 Mechanical properties of the material

Yield point (N/mm <sup>2</sup> )		Tensile strength (N/mm <sup>2</sup> )	Yield ratio (%)	Uniform elongation (%)
Upper	Lower			
502	494	637	78.9	9.5
(440–540)	–	(590–740)	(≤80)	–

( ) The values in parentheses represent the specification requirements

test of steel components. The proposed model is examined by comparing with test results. In addition, a series of numerical analysis of cantilever beam with parameters of steel grades and loading histories is conducted to show the example of application of the proposed model.

## 2 Cyclic Loading Test of 590 N/mm<sup>2</sup> Grade High Performance Steel SA440

### 2.1 Specimen

The shape of the specimen is shown in Fig. 1. Material of the specimens is 590 N/mm<sup>2</sup> grade high performance steel SA440 for building construction (JISF 2004). The specimens were made from a same plate, followed the rolling direction. Length and diameter of the testing area are 17 mm and 8 mm, respectively. Radius of the fillet is 10 mm.

Mechanical properties of the material obtained by coupon test conducted with JIS 14A type specimen (JIS Z2411 2011) are summarized in Table 1. The stress–strain relationship is shown in Fig. 2. Chemical composition of the material is listed in Table 2.

### 2.2 Testing Procedure

The test set-up is shown in Fig. 3. In this study, cyclic loading tests were conducted under quasi-static condition at a loading rate of 0.20 mm/min (about 0.01%/s strain rate) using a mechanical type universal testing machine of which the loading capacity is 500 kN. The loading histories adopted in this study are summarized in Table 3. Those consist of two types of incremental strain amplitude

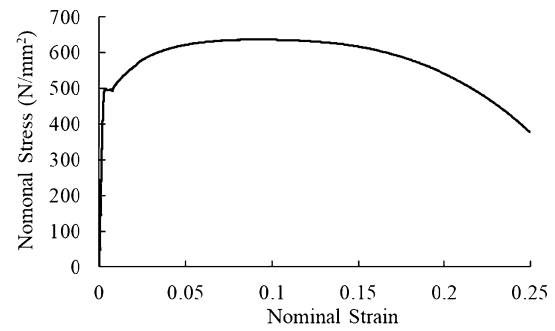


Fig. 2 Stress–strain relationship of the material (Coupon test result)

Table 2 Chemical composition of the material

C (%)	Si (%)	Mn (%)	P (%)	S (%)
0.10	0.26	1.44	0.008	0.001
(≤0.18)	(≤0.55)	(≤1.60)	(≤0.020)	(≤0.008)

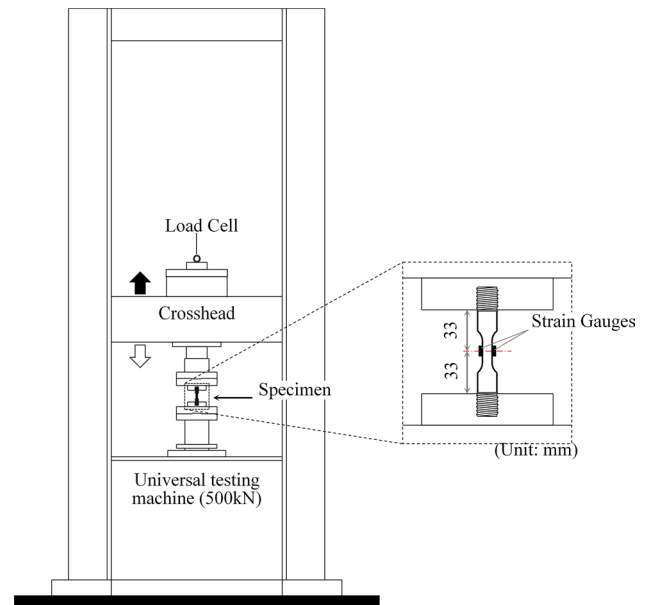


Fig. 3 Test set-up

and one programmed strain amplitude were set within the range of which buckling does not occur. The programmed strain amplitude is shown in Fig. 4, which is composed with both large and small strain amplitudes and takes into consideration the eccentricity of symmetry axes of the strain amplitudes.

As for the measurement, the imposed axial force to the specimens was measured by a load cell installed in the crosshead. The nominal stress  $n\sigma$  was obtained by dividing axial force with original cross-sectional area. The nominal strain of the parallel testing section  $n\epsilon$  was measured with a couple

**Table 3** List of the loading histories

Specimen	Loading histories
SA440_0.5	±0.5% incremental strain amplitude (2 cycles at each amplitude)
SA440_1.0	±1.0% incremental strain amplitude (2 cycles at each amplitude)
SA440_P	Programmes strain amplitude (shown in Fig. 4)



**Fig. 4** Programmed loading history (Specimen SA440\_P)

of strain gauges glued to both sides of the section in parallel testing section. Measured nominal strain was used to control the loading histories.

### 2.3 Test Results

The hysteretic model proposed in this study is expressed in true stress  $t\sigma$ —true strain  $t\varepsilon$  relationship. So,  $t\sigma$  and  $t\varepsilon$  are converted from  $n\sigma$  and  $n\varepsilon$  assuming constant volume by Eqs. (1) and (2). Obtained  $n\sigma$ – $n\varepsilon$  relationships and  $t\sigma$ – $t\varepsilon$  relationships of each specimens are shown in Fig. 5.

$$t\sigma = (1 + n\varepsilon) \cdot n\sigma \tag{1}$$

$$t\varepsilon = \ln(1 + n\varepsilon) \tag{2}$$

## 3 Hysteretic Model of 590 N/mm<sup>2</sup> Grade High Performance Steel SA440

### 3.1 Decomposition of Hysteresis Curve

The hysteresis curve under cyclic loading of steel material can be decomposed into the skeleton part, the Bauschinger part and the elastic unloading part as shown in Fig. 6. The skeleton curve is formed by sequentially connecting the paths of the loads that exceed the maximum load attained in the preceding cycle. The Bauschinger parts are defined softened part due to the Bauschinger effect. In the Fig. 6,  $\sum \Delta\varepsilon$  is the cumulative plastic strain in skeleton curve, and

$\Delta\varepsilon_B$  is the increment of plastic strain in Bauschinger part in each cycle.

### 3.2 Modelling of the Hysteresis Curve

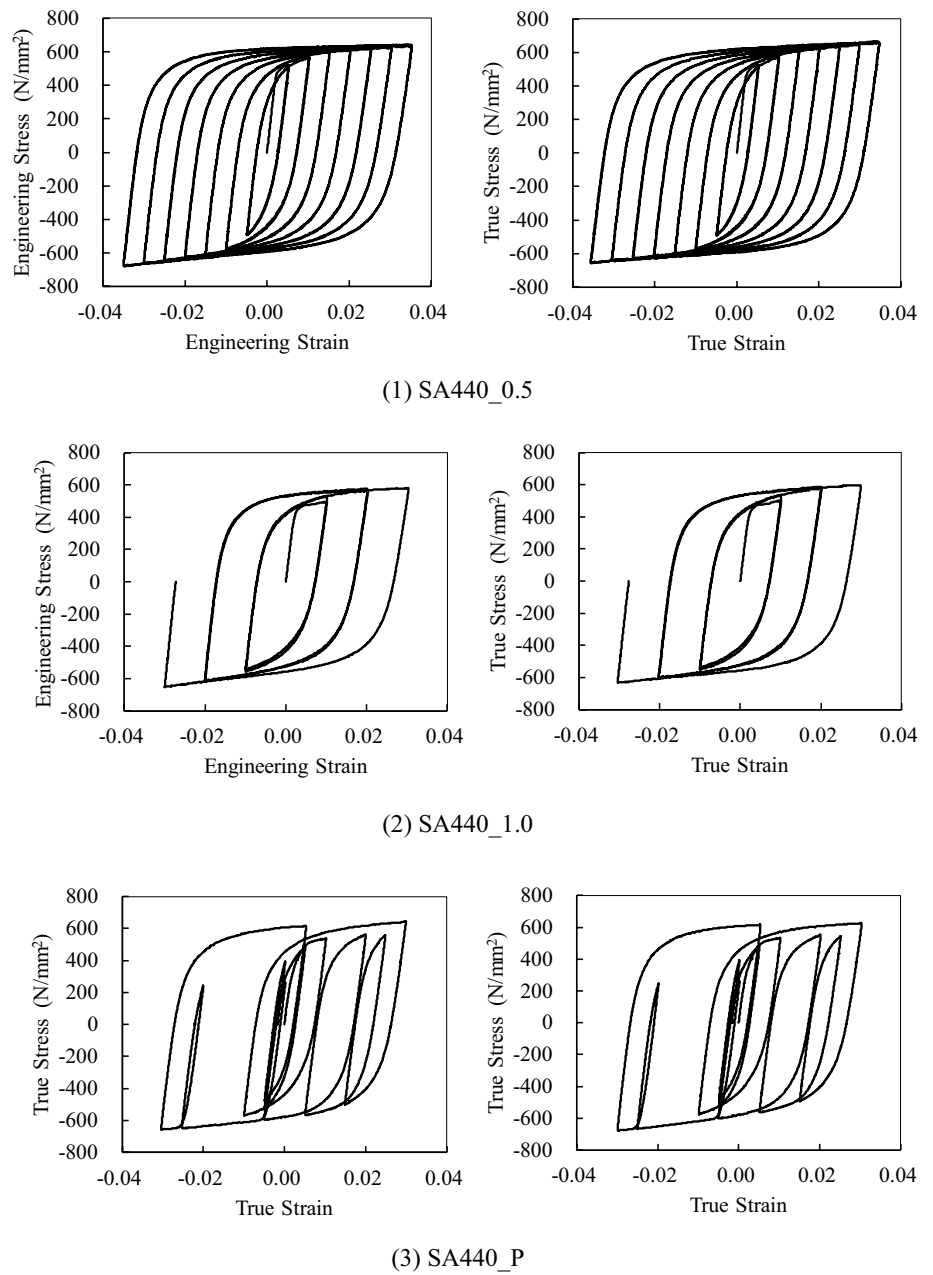
As for the skeleton curve, it is empirically known that it corresponds to the stress–strain relationship obtained by monotonic loading test (Kato et al. 1970, 1973; Akiyama 1985). In addition, skeleton curve of the true-stress true strain relationships in the compression side and the tension side exhibits symmetric relation. In this study, the skeleton curve in the hysteretic model is adopted as true stress–true strain relationship converted from the nominal stress–nominal strain relationship of coupon test by Eqs. (1) and (2).

As for the Bauschinger part, it is empirically known that it can be modeled as a bi-linear model in the hysteresis curve of the structural steel material, and the plastic strain of that relates to the cumulative strain in the skeleton curve experienced so far (Akiyama et al. 1995; Yamada and Jiao 2016). In this study, the Bauschinger part is modeled as a bi-linear model with the stress when entering the skeleton curve  $t\sigma_{Bs}$ , elastic stiffness  $E$ , plastic strain increments in each cycle of the Bauschinger part  $\Delta_t\varepsilon_B$ , and stress of the stiffness changing point  $t\sigma_E$ .

Among them, the stress when entering the skeleton curve  $t\sigma_{Bs}$  can be set as the maximum stress from the previous cycle. On the other hand, plastic strain increments in the Bauschinger parts in each cycle  $\Delta_t\varepsilon_B$  and stress of the stiffness changing point  $t\sigma_E$  are evaluated based on the test results. The relationship between plastic strain increments in the Bauschinger parts in each cycle  $\Delta_t\varepsilon_B$  and cumulative strain in the skeleton curve  $\sum \Delta\varepsilon$  are shown in Fig. 7 with previous test results of 400 N/mm<sup>2</sup> grade structural steel (Yamada and Jiao 2016). As shown in Fig. 7, the two variables exhibit a linear relationship and a simple linear Eq. (3) is obtained for 590 N/mm<sup>2</sup> grade high performance steel SA440. From Fig. 7, it is confirmed that constant in the relationship  $\Delta_t\varepsilon_B$  and  $\sum \Delta\varepsilon$  is different according to the steel grade, and SA440 steel shows more plastic deformation in the Bauschinger part under cyclic loading than 400 N/mm<sup>2</sup> grade structural steel.

$$\Delta_t\varepsilon_B = 0.72 \sum \Delta_t\varepsilon_s \tag{3}$$

**Fig. 5** True stress and true strain relationships of each specimen



Coefficient  $\alpha_B$ , is defined as the ratio of stress of the stiffness changing point  ${}_t\sigma_E$  to the stress when entering the skeleton curve  ${}_t\sigma_{Bs}$ .  $\alpha_B$  is obtained by matching the  ${}_t\sigma_{Bs}$  of the bi-linear model to dissipate equivalent energy with the Bauschinger part of the test results as shown in Fig. 8. Here, initial stiffness of the bi-linear model is the elastic stiffness.  $\alpha_B$  in each cycles of the Bauschinger part are shown in Fig. 9 in the relationship with the increments of plastic strain in the Bauschinger part  $\Delta\varepsilon_B$ . In Fig. 9, previous test results of 400 N/mm<sup>2</sup> grade structural steel (Yamada and Jiao 2016) are also plotted. As for  $\alpha_B$ , same model with 400 N/mm<sup>2</sup> grade structural steel is adopted.

$$\alpha_B = 0.67 \tag{4}$$

### 3.3 Hysteretic Model

Details of the hysteretic model are expressed in the previous paper (Yamada and Jiao 2016). Here, for understanding, an example (tensile start) of the hysteresis is shown in Fig. 10. It can be summarized as follows.

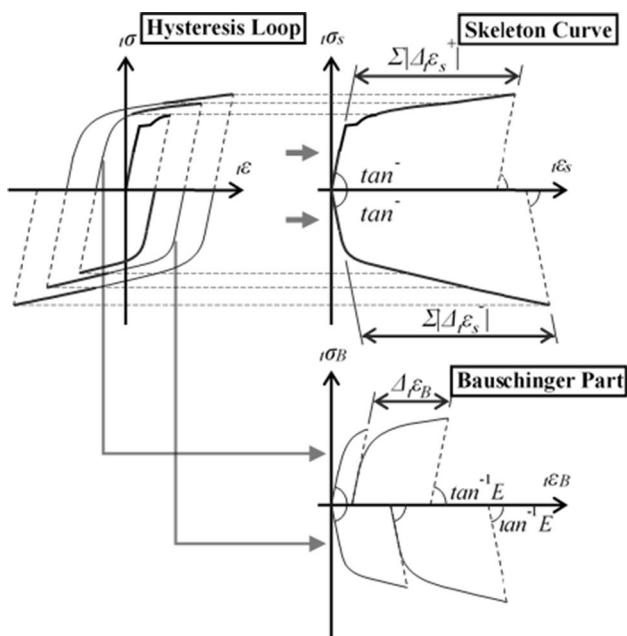


Fig. 6 Decomposition of the hysteresis curve

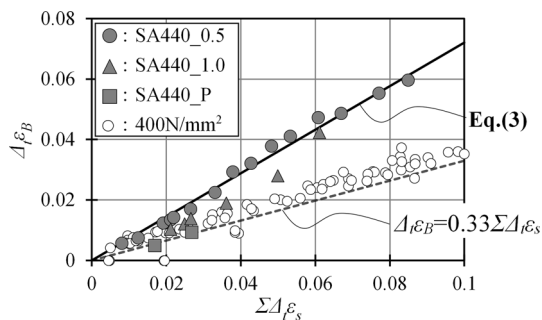


Fig. 7 Relationship between  $\Delta_t \epsilon_B$  and  $\Sigma \Delta \epsilon$

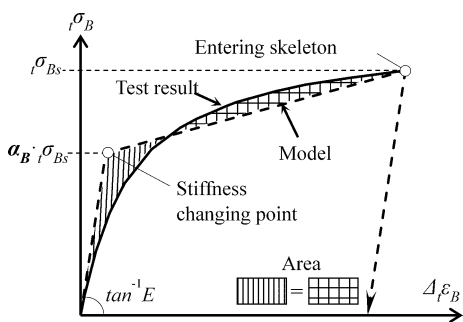


Fig. 8 Modeling of the Bauschinger part

- Compressive side of the first cycle is taken as the skeleton curve due to the compressive stress first experienced by the steel material (3–6 in Fig. 10). Although softening caused by experiencing of plastic strain in the tensile side

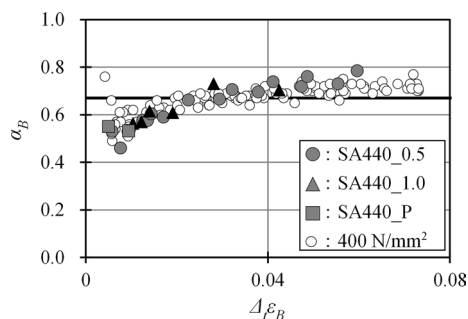


Fig. 9 Relationship between  $\alpha_B$  and  $\Delta \epsilon_B$

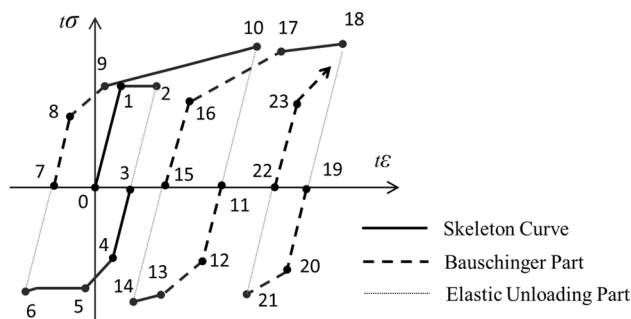


Fig. 10 Example of the hysteretic model considering the Bauschinger effects

is considered by adopting bi-linear model of the Bauschinger part (4–5 in Fig. 10).

- The entering point to the skeleton curve and the unloading point in the skeleton curve are reset every time if and only if the hysteresis loop enters its skeleton curve and remain unchanged until the hysteresis loop enters next skeleton curve fragment. (loops 0–2, 3–6, 7–10, 11–14 and 15–18 in Fig. 10).
- The true strain increment from the stiffness changing point in the Bauschinger Part to the next entering point to the skeleton curve (8–9, 12–13, 16–17 in Fig. 10) is calculated by Eq. (3).
- Stress of the stiffness changing point of the Bauschinger part  $t \sigma_{Bs}$  is determined by experienced peak stress in the skeleton curve and Eq. (4). (points 8, 12, 16, 20 and 23 in Fig. 10).
- The case of unloading within the plastic region of the Bauschinger part. Before unloading, the plastic region heads to the next entering skeleton point (23- in Fig. 10, which heads to point 18).

### 3.4 Comparison of Hysteretic Model and Test Results

Comparison of the hysteretic model and test results are shown in Figs. 11 and 12. Figure 11 are the comparison of

**Fig. 11** Comparison of the hysteretic model and the test result

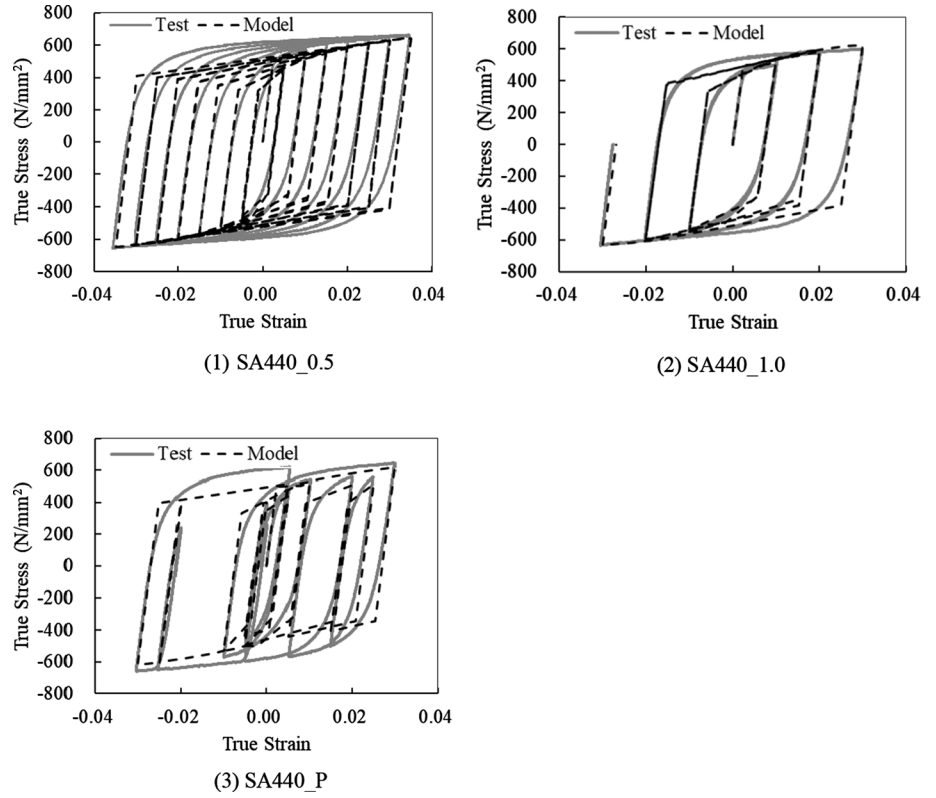
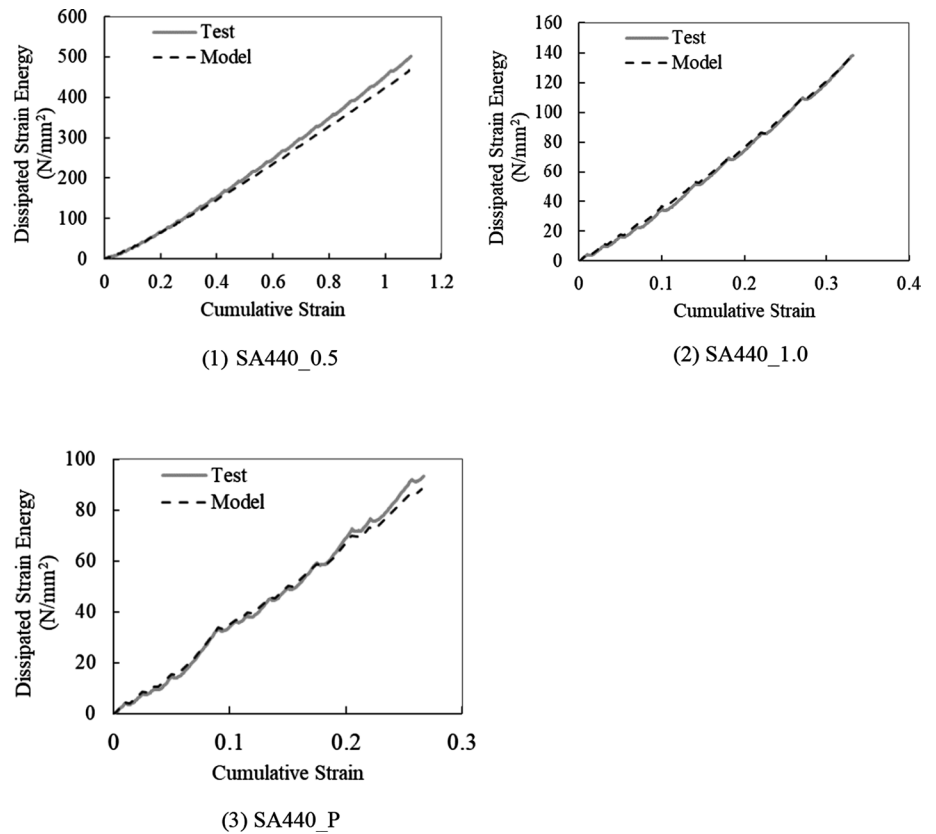


**Fig. 12** Comparison of the dissipated strain energy and cumulative strain relationships



the stress–strain relationships. Figure 12 are the comparison of the dissipated strain energy and cumulative strain relationships. The gray lines and the black broken lines represent the test results and the hysteretic model subjected to the same strain histories of the test, respectively. With the bilinear model, some tolerable error can be found with the stress–strain relationships, while the dissipated strain energy and cumulative strain relationship results show very good accuracy. According to Fig. 8, the main principle of the modelling is using a bilinear relationship to provide equivalent energy dissipation with the real hysteretic loops. The overall performance of the proposed hysteretic model of 590 N/mm<sup>2</sup> grade high performance steel for building construction is satisfactory.

### 4 Example of Application on Member Analysis

To show the effectiveness of the proposed hysteretic model of 590 N/mm<sup>2</sup> grade high performance steel for building construction, a series of numerical analysis is conducted. Target of analysis is a cantilever beam with welded connection at the fixed end side as shown in Fig. 13. The cross section is H-600×200×11×17, and the span is 3 m. Parameters are steel grades and loading histories as summarized in Table 4. As for the hysteretic model of steel material, proposed model in this study and proposed model in previous study (Yamada and Jiao 2016) are adopted for SA440 and SN400 steel, respectively.

Analysis is concocted with in-plane analysis method as previous study (Yamada and Jiao 2016). That is, the moment curvature relationship ( $M-\phi$ ) of a certain beam section is derived through the internal force balance under the assumption of the plane section. Additionally, the load-deformation relationship ( $M-\theta$ ) of the beam is derived by integrating the moment–curvature relationship along the beam span.

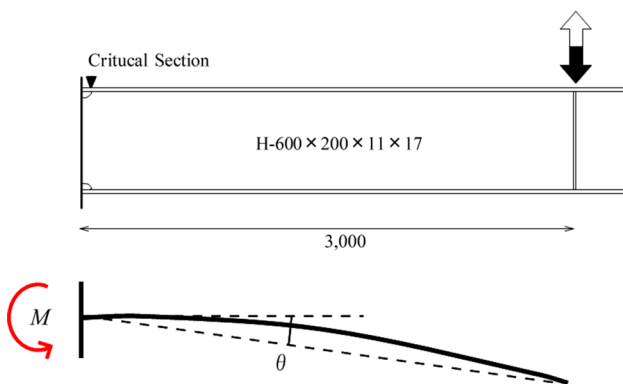


Fig. 13 Cantilever beam for the analysis

Table 4 List of parameters of the analysis

Steel		Loading history
SA440	×	Monotonic loading
		Constant amplitude [ $\pm 0.01$ (rad)] cyclic loading
SN400		Constant amplitude [ $\pm 0.02$ (rad)] cyclic loading
		Constant amplitude [ $\pm 0.03$ (rad)] cyclic loading

Both Hysteretic models for SA440 and SN400 are concise but consider not only difference of the plastic range and the strain hardening range, but also the Bauschinger effect. Therefore, the analysis results reflect the realistic behaviors of the steel material. Figure 14 shows comparison of the relationships between moment at beam end  $M$  and rotation angle of beam  $\theta$  and comparison of the relationships between nominal strain at the flange of the critical section  $n\epsilon_f$  and  $\theta$ , under monotonic loading. Here, the critical section is a cross section at the position of the toe of the weld access hole that is the starting point of the fracture. Figure 15 shows comparison of the relationships between  $M$  and  $\theta$  and comparison of the relationships between  $n\epsilon_f$  and cumulative rotation angle  $\sum [\Delta\theta]$ , under cyclic loading.

In case of monotonic loading, around  $\theta$  of 0.02 (rad), flange strain of the critical section is almost same in SN400 and SA440. On the other hand, in case of cyclic loading with amplitude of 0.02 (rad), strain of the flange in the critical section of SN400 is smaller than that of SA440, in the peak of 2nd and subsequent cycles. This is because

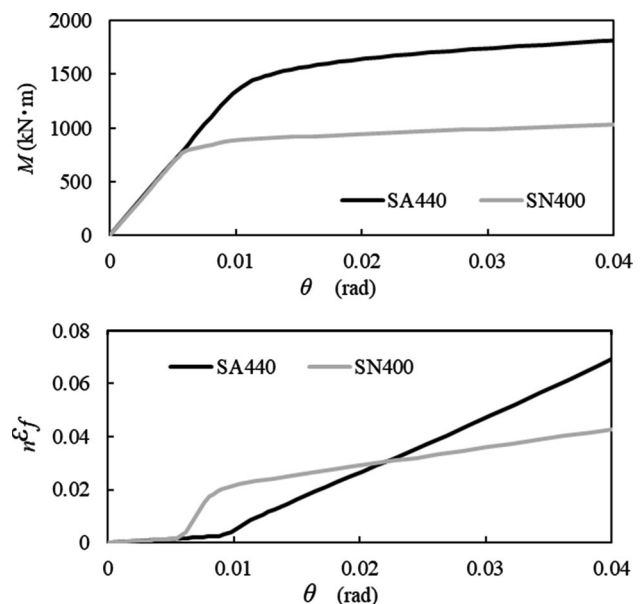
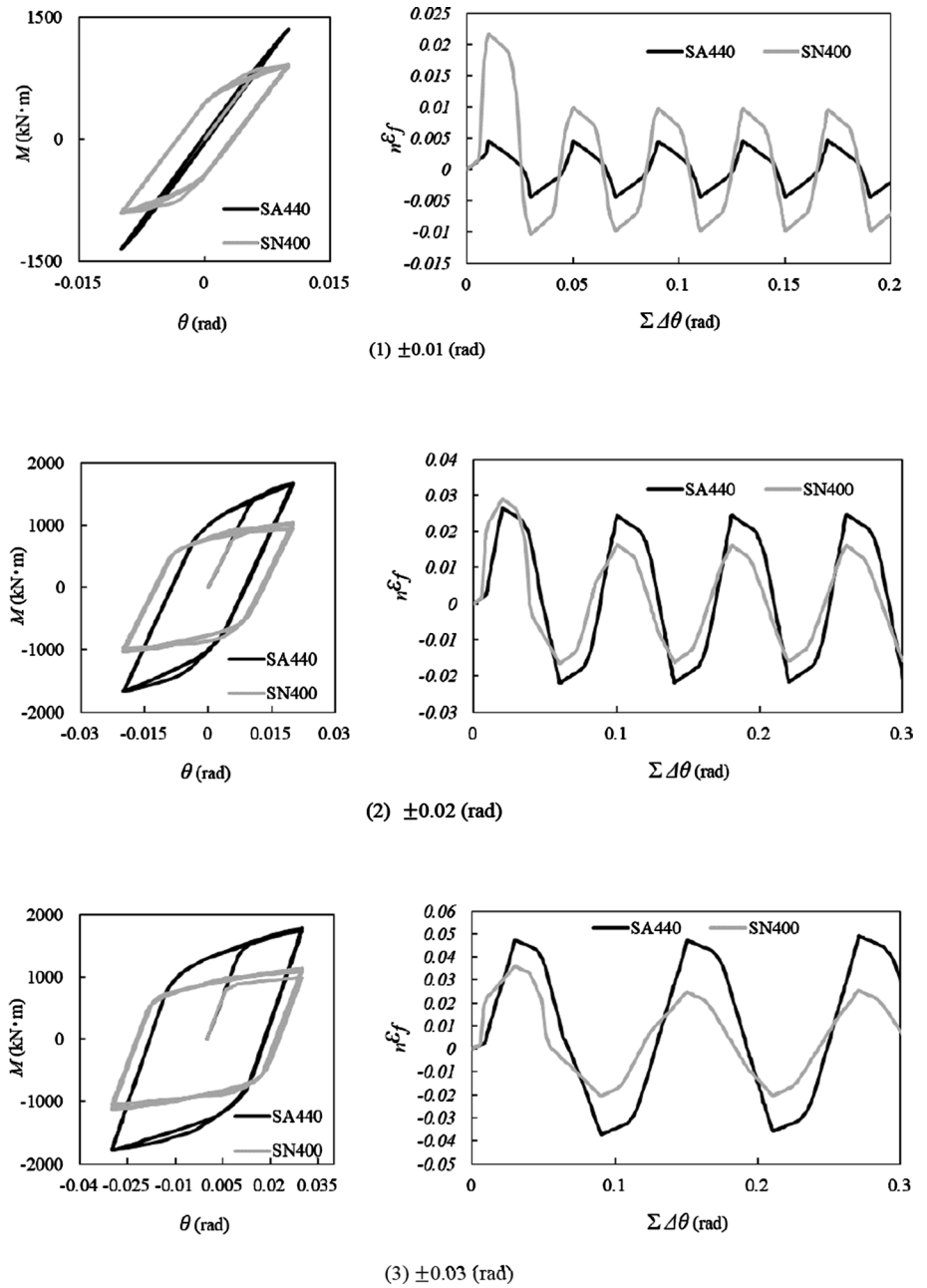


Fig. 14  $M-\theta$  relationships and  $n\epsilon_f-\theta$  relationships under monotonic loading

**Fig. 15**  $M$ – $\theta$  relationships and  $n\varepsilon_f$ – $\Sigma[\Delta\theta]$  relationships under cyclic loading



of the plastic region in the stress–strain relationship on the positive behavior of monotonic loading and 1st cycle of cyclic loading. Also, in cyclic loading with yielding, there is a difference in the shape of the history between the first cycle on the negative side and the 2nd and subsequent cycles. This is the effect of the Bauschinger part of the stress–strain relationship. The effect of the Bauschinger part is found not only in the  $M$ – $\theta$  relationship but also in the strain history in each part of members. By using a realistic hysteretic model of a steel material, it is possible to evaluate the strain history of the flange in the critical section under cyclic loading and expect to contribute

to evaluate the effect of the steel type on the Low Cycle Fatigue Life of members.

### 5 Conclusion

A concise hysteretic model of 590 N/mm<sup>2</sup> grade high performance steel for building construction (SA440) is proposed based on the test results of axial cyclic loading test. The proposed model is basically same with hysteretic model for 400 N/mm<sup>2</sup> grade structural steel proposed in previous study (Yamada and Jiao 2016), and it composed of the skeleton



curve, the Bauschinger part and the elasticity unloading part. Here, the skeleton curve is based on the coupon test results and the Bauschinger part is simplified as a bilinear model which is a function of the cumulative strain in the skeleton curve the material has experienced so far. In comparison with test results, the proposed model shows good correspondence, especially in energy dissipation.

In addition, to examine the effectiveness of the proposed model, a series of numerical analysis of cantilever beam with parameters of steel grade and loading histories is conducted. From analytical results, it is clarified that, difference of the structural behavior and the strain history in members due to the difference of stress–strain relationship characteristics of steel material can be examined by using the proposed hysteretic models.

**Acknowledgements** Steel Material used in this study is supplied by the Japan Iron and Steel Foundation.

**Author Contributions** All authors contributed to the study conception, design, experiments and the discussion.

## Appendix: In-Plane Analysis of Steel Beam-to-Column Connections

### Basic Assumptions

The in-plane analysis of the ideal cantilever wide-flange beams subjected to cyclic loading histories was conducted under the following assumptions:

- (1) The assumption of the plane section.
- (2) The deformation due to shear force is considered to be always elastic.
- (3) There is no out-of-plane deformation of the beam.
- (4) The beam reaches its maximum load without local buckling.

### Analytical Algorithm

The algorithm of this analysis is based on the monotonic in-plane analyses in Kato et al. (1966), Yamada et al. (1966) and Yamada and Akiyama (1995). The basic idea of the algorithm is to obtain the moment–curvature relation ( $M-\varphi$ ) of a certain beam section through the internal force balance under the assumption of the plane section. Additionally, the load–deformation relation ( $M-\theta$ ) of the beam can be derived by integrating the moment–curvature relation along the beam span. This analytic method is known to be sufficiently accurate before the beam reaches its maximum strength.

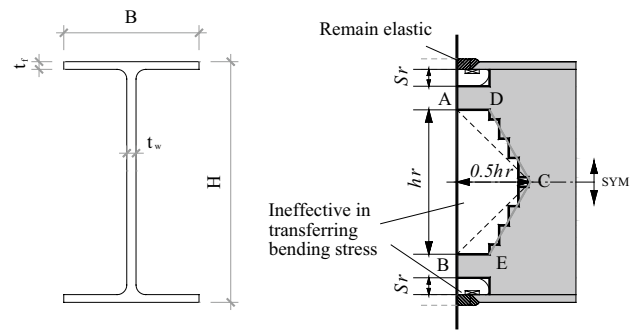


Fig. 16 Analytical model of beam-end

### Modeling of the Connection Details

In the WF composite beam connected to RHS column that is commonly used in Japan, ductile fracture occurs mostly due to the decrease of the web's joint efficiency and the strain concentration on the bottom flange. The simulation of the connection details is a very important issue in the beam analysis. The loss of beam section due to the weld access holes and the local out-of-plane bending of the tube wall of the RHS column cause the strain concentration at the beam-end flange, which directly leads to the early fracture (Matsumoto et al. 2000). The joint efficiency of the beam web at the connection is reduced (the beam-to-column connection's moment transmission capacity is less than 100%). To simulate this phenomenon, the analytical model of the in-plane beam analysis took into consideration the decrease of the joint efficiency.

The analysis model of beam-end is shown in Fig. 16. Two rectangles at the location of the weld access holes, with the length of each side equals to the length of the weld access hole along the beam height and the length of the weld access hole along the beam span respectively, should also be set to be ineffective in carrying the bending stress. Note here, shear force is carried by the net beam section without weld access holes. Moreover, comparing with the beam flange, the strength of the diaphragms and the full-penetrated weld area is considered to be much higher. In the cyclic in-plane beam analysis, these parts were assumed to be always elastic.

### References

- Akiyama, H. (1985). *Earthquake-resistant limit-state design for buildings*. Tokyo: University of Tokyo Press.
- Akiyama, H., Takahashi, M., & Shi, Z. (1995). Ultimate energy absorption capacity of round-shape steel rods subjected to bending. *Journal of Structural and Construction Engineering, Architectural Institute of Japan*, 475, 145–154. (in Japanese).

- JIS (Japanese Industrial Standard) G3101. (2010). Rolled steels for general structure.
- JIS G3136. (2012). Rolled steels for building structure
- JIS Z2411. (2011). Metallic materials-tensile testing-method of test at room temperature.
- JISF (the Japan Iron and Steel Foundation). (2004). High performance 590 N/mm<sup>2</sup> steel for building structures (SA440). JISF Specification No. MDCR 0013-2004 (**in Japanese**).
- Kato, B., Akiyama, H., & Uchida, N. (1966). Ultimate strength of structural steel members. *Transactions of the AIJ*, 119, 22–30. (**in Japanese**).
- Kato, B., Akiyama, H., & Yamanouchi, Y. (1973). Predictable properties of material under incremental cyclic loading. In *Proceedings of LABSE symposium on resistance and ultimate deformability of structures acted on by well defined repeated loads* (pp. 119–124).
- Kato, B., Aoki, H., & Yamanouchi, H. (1970). Experimental study on the behavior of steel material under tension and compression loadings. In *Proceedings of annual meeting of the Architectural Institute of Japan* (**in Japanese**).
- Matsumoto, Y., Yamada, S., Akiyama, H. (2000). Fracture of beam-to-column connections simulated by means of the shaking table test using the inertial loading equipment. In *Behaviour of steel structures in seismic areas* (pp. 215–22). Rotterdam: Balkema.
- Menegotto, M., & Pinto, P. E. (1973). Method of analysis for cyclically loaded R. C. plane frames including changes in geometry and non-elastic behavior of elements under combined normal force and bending. In *Proceedings of LABSE symposium on resistance and ultimate deformability of structures acted on by well defined repeated loads* (pp. 15–22).
- Ramberg, W., & Osgood, W. R. (1943). Description of stress–strain curves by three parameters. Technical Notes 902, National Advisory Committee for Aeronautics.
- Yamada, M., Sakae, K., Tadokoro, T., & Shirakawa, K. (1966). Elastoplastic bending deformation of wide flange beam-columns under axial compression, part I: Bending moment-curvature and bending moment-deflection relations under static loading. *Journal of Structural and Construction Engineering, Transactions of the AIJ*, 127, 8–14. (**in Japanese**).
- Yamada, S., & Akiyama, H. (1995). Deteriorating behavior of steel members in post-buckling range. In *Structural stability and design* (pp. 169–74). Rotterdam: Balkema.
- Yamada, S., & Jiao, Y. (2016). A concise hysteretic model of structural steel considering the Bauschinger effect. *International Journal of Steel Structures*, 16(3), 671–683. <https://doi.org/10.1007/s13296-015-0134-9>.

**Publisher's Note** Springer Nature remains neutral with regard to jurisdictional claims in published maps and institutional affiliations.